



OPEN

# SGOL1 variant B induces abnormal mitosis and resistance to taxane in non-small cell lung cancers

SUBJECT AREAS:  
NON-SMALL-CELL LUNG  
CANCER  
BIOMARKER RESEARCH

Received  
1 May 2013

Accepted  
2 October 2013

Published  
22 October 2013

Correspondence and  
requests for materials  
should be addressed to  
H.S. (hsugimur@hama-  
med.ac.jp)

Shun Matsuura<sup>1,2</sup>, Tomoaki Kahyo<sup>1</sup>, Kazuya Shinmura<sup>1</sup>, Moriya Iwaizumi<sup>1</sup>, Hidetaka Yamada<sup>1</sup>, Kazuhito Funai<sup>3</sup>, Jun Kobayashi<sup>4</sup>, Masayuki Tanahashi<sup>5</sup>, Hiroshi Niwa<sup>5</sup>, Hiroshi Ogawa<sup>6</sup>, Takashi Takahashi<sup>7</sup>, Naoki Inui<sup>2</sup>, Takafumi Suda<sup>2</sup>, Kingo Chida<sup>2</sup>, Yoshinori Watanabe<sup>8</sup> & Haruhiko Sugimura<sup>1</sup>

<sup>1</sup>Department of Tumor Pathology, Hamamatsu University School of Medicine, 1-20-1 Handayama, Higashi-ku, Hamamatsu, Shizuoka, 431-3192, Japan, <sup>2</sup>Second Division, Department of Internal Medicine, Hamamatsu University School of Medicine, 1-20-1 Handayama, Higashi-ku, Hamamatsu, Shizuoka, 431-3192, Japan, <sup>3</sup>First Department of Surgery, Hamamatsu University School of Medicine, 1-20-1 Handayama, Higashi-ku, Hamamatsu, Shizuoka, 431-3192, Japan, <sup>4</sup>Thoracic Surgery, Shimada Municipal Hospital, 1200-5 Noda, Shimada, Shizuoka, 427-8502, Japan, <sup>5</sup>Division of Thoracic Surgery, Respiratory Disease Center, <sup>6</sup>Division of Pathology, Seirei Mikatahara General Hospital, 3453 Mikatahara, Kita Ward, Hamamatsu, Shizuoka, 433-8558, Japan, <sup>7</sup>Department of Molecular Carcinogenesis, Nagoya University Graduate School of Medicine, 65 Tsurumai-cho, Showa-ku, Nagoya, Aichi, 466-8550, Japan, <sup>8</sup>Laboratory of Chromosome Dynamics, Institute of Molecular and Cellular Biosciences, University of Tokyo, Yayoi, Tokyo, 113-0032, Japan.

**Mitosis is the most conspicuous cell cycle phase and Shugoshin-like 1 (SGOL1) is a key protein in protecting sister chromatids from precocious separation during mitosis. We studied the role of SGOL1 and its splice variants in non-small cell lung cancer (NSCLC) using 82 frozen NSCLC tissue samples. SGOL1-B expression was prevalent in smokers, in cases with a wild-type (WT) EGFR status, and in cases with the focal copy number amplification of genes that are known to be important for defining the biological behaviors of NSCLC. The overexpression of SGOL1-B1 in an NSCLC cell line induced aberrant chromosome missegregation, precociously separated chromatids, and delayed mitotic progression. A higher level of SGOL1-B mRNA was related to taxane resistance, while the forced downregulation of SGOL1-B increased the sensitivity to taxane. These results suggest that the expression of SGOL1-B causes abnormal mitosis and taxane resistance in NSCLC cells.**

**S**hugoshin-like protein (SGOL1), one of the human homologs of yeast shugoshin, is localized in the centromeric region and prevents the precocious cleavage of the cohesion complex at the centromere<sup>1</sup>. SGOL1 is crucial for mitotic progression and chromosome segregation. In a study on human cancer, we found that SGOL1 expression was decreased in colorectal cancer and that SGOL1-knockdown led to chromosome instability (CIN) in a colon cancer cell line<sup>2</sup>. In general, many tumor-specific splicing variants have been studied in a variety of tumors. SGOL1 variants have been previously identified, and these variants appear to have a negative effect on the cohesion between sister chromatids<sup>3</sup>, with SGOL1-P1 causing abnormal mitosis and unstable chromatid cohesion in colon cancer<sup>4</sup>. However, the role of SGOL1 splice variants in human cancer is generally unknown.

Lung cancer is a leading cause of cancer mortality in many countries<sup>5</sup>. Detailed molecular and biological characterization of certain types of NSCLC has provided better guidance in clinical management<sup>6–8</sup>, that is, targeted therapies and individualized treatments. Taxanes (*e.g.*, docetaxel and paclitaxel), disrupters of microtubule, are commonly used for the treatment of advanced NSCLC<sup>9</sup>. The efficacy of taxanes against cancer cells can be attributed to mitotic arrest resulting in mitotic catastrophe, promoting cell death during metaphase or death preceded by multinucleation<sup>10</sup>. However, the strategies that resistant tumor cells use to evade death induced by taxanes are also unclear. The cell machinery involved in mitosis control may be involved in taxane resistance of cancer cells.

In this study, we evaluated the expression levels of SGOL1 mRNA in clinical NSCLC specimens and investigated the malfunction of SGOL1-B, a tumor-specific variant, in NSCLC cells. Furthermore, we investigated whether the SGOL1-B expression level defines the response of NSCLC cells to taxanes.



## Results

**Increased SGOL1-B expression in NSCLC.** To investigate the status of SGOL1 expression in NSCLC tissues, the mRNA level of SGOL1 was quantified using real-time RT-PCR with primers covering the SGOL1-A, -B, and -C splicing variants (Figures 1a and b) in 82 pairs of primary NSCLC and matched normal tissues located adjacent to the carcinoma. Increased SGOL1 expression ( $T > N$ ) was observed in 62 (75.6%) of the 82 NSCLCs (Figure 1c); moreover, a significant difference was detected in the mRNA expression level of SGOL1 between cancerous and non-cancerous tissue using a statistical analysis ( $P < 0.0001$  according to a Wilcoxon matched pairs test). This result suggests that SGOL1 expression is upregulated in NSCLC.

Since several splicing variants of SGOL1 exist (Figure 1a), we next examined whether the mRNA expression of each SGOL1 variant was upregulated in the 82 NSCLCs. We compared the expression level of each SGOL1 variant in matched pairs of cancerous and non-cancerous tissues. A paired comparison in all cases revealed a statistically significant increase in the expression of SGOL1-B, but not of SGOL1-A or SGOL1-C, in the cancerous tissue, compared with the non-cancerous tissues (Figure 1d,  $P = 0.047$ ). Very interestingly, all the cancers expressing SGOL1-B ( $n = 24$ ) showed increased expression levels in the cancerous tissue, compared with the non-cancerous tissue (cancer tissue-specific expression). We analyzed the contributions of other SGOL1 isoforms to the phenotype exerted by SGOL1-B1 expression. In SGOL1-B expressing cases, the ratio SGOL1-A/SGOL1-B is larger than 1.0 while SGOL1-C/SGOL1-B is lower than 1.0 (Supplementary Table S1 online). These results suggest that SGOL1-B has an important role in the carcinogenesis of NSCLC; therefore, we focused on SGOL1-B in the subsequent studies.

**Association of SGOL1-B expression with EGFR status and focal copy number amplifications in NSCLC.** Next, we investigated whether the levels of SGOL1-B mRNA expression were associated with the clinicopathological features in NSCLC patients (Table 1). The frequencies of patients with smoking history and WT EGFR were statistically higher in the group with SGOL1-B-positive cancer than in the group with SGOL1-B-negative cancer ( $P = 0.029$  and  $P = 0.017$ , respectively). No associations were found between the clinicopathological factors of sex, onset age, tumor pathology, or tumor stage and the status of SGOL1-B mRNA expression in the cancerous tissue.

Then, we hypothesized that SGOL1-B-positive lung cancers may have more frequent and extensive genomic alterations. To assess the association between SGOL1-B expression and genetic alterations, we selected five DNA targets commonly amplified in lung cancer, i.e., 8p12 (FGFR1), 3q26.3-q27 (SOX2 and PIK3CA), 7q31.1 (MET), and 7p12 (EGFR), and evaluated their gene copy changes using FISH in a tissue microarray<sup>11–15</sup>. A specific relationship was not observed between SGOL1-B expression and focal copy number amplification at a particular locus, but focal copy number amplifications at one of these loci were identified in 18 of the 58 (31.0%) patients with SGOL1-B negative cancer and in 13 of the 24 (54.2%) patients with SGOL1-B positive cancer ( $P = 0.049$ , Table 1). The mechanisms of these focal copy number amplifications are not known, but SGOL1-B-positive cancer represents a subset of lung cancers with focal copy number amplifications.

**SGOL1-B1 is localized at centromeres, and SGOL1-B1 overexpression exhibits aberrant chromosome-alignment during mitosis in lung cancer cells.** To characterize the effect of SGOL1-B expression in NSCLC, the lung adenocarcinoma cell line ACC-LC-176 was transfected with an expression vector for MYC-tagged SGOL1-B1. The overexpression of MYC-SGOL1-B1 was confirmed in ACC-LC-176 cells using a western blot analysis (Figure 2a). An immunofluorescence analysis revealed that SGOL1-B1 was localized in the nucleus during interphase and mitosis (Figure 2b). To further investigate the

specific localization of SGOL1-B1, we performed a co-immunofluorescence study for the centromere and MYC-SGOL1-B1. MYC-SGOL1-B1 was clearly localized at the centromere in SGOL1-B1-overexpressing cells (Figure 2c). Furthermore, when we focused on the chromosome positioning morphology during mitosis, chromosome missegregation in pro-metaphase was more frequently observed in SGOL1-B1-overexpressing cells than in empty-vector transfected cells (66.7% vs. 6.8%) (Figure 2c). These results suggested that SGOL1-B1 overexpression is associated with mitotic abnormalities. Furthermore, we tested to see if the overexpression of SGOL1-A1 rescued the phenotype induced by the overexpression of SGOL1-B1. The chromosome missegregation induced by SGOL1-B1 was partially dismissed in the presence of SGOL1-A1 (Figure 2d). Since multiple spindle poles have been reported to be common in mitotic SGOL1-knockdown cells (1), we examined the cells for the presence of centrosome amplification (an extra centrosome; more than 3 centrosomes). Centrosome amplification was observed more frequently in the ACC-LC-176 cells expressing SGOL1-B1 than in the vector control cells (Figure 2e). All these results suggested that SGOL1-B1 is localized at the centromere and that the overexpression of SGOL1-B1 exhibits aberrant chromosome-alignment in lung cancer cells.

**Cohesion defect and mitotic progression delay in lung cancer cells expressing SGOL1-B1.** SGOL1 is recognized as a centromeric protector in somatic cells during mitosis (1). To assess the effect of SGOL1-B1 on sister chromatid cohesion in lung cancer cells, a chromosome spread assay was performed in the ACC-LC-176 cell line. Spread chromosomes were stained with DAPI, and the frequency of each of the separation patterns was counted (Figure 3a). As a positive control for this experiment, SGOL1 knockdown was also performed using shRNA plasmids targeting SGOL1-A, SGOL1-B, and SGOL1-C, as reported previously (3). Severe cohesion defects were observed significantly more frequently in SGOL1-B1-expressing cells (22%) and SGOL1-knockdown cells (31%) than in control cells (7%) (Figure 3b). These results suggest that SGOL1-B induces the precocious separation of sister chromatids in lung cancer cells. We next monitored the mitotic progression in SGOL1-B1-expressing ACC-LC-176 cells, SGOL1-knockdown cells, and control cells using time-lapse microscopy. The chromosomal masses separated without congressing at the metaphase plate in some percentage of the SGOL1-B1-transfected cells and SGOL1-knockdown cells; however, no such cells were observed in empty vector-transfected cells (Figure 3c and Supplementary Movie 1–3 online). We measured the time from nuclear envelop breakdown (NEBD) to the anaphase transition. The median time was 33.1 minutes in the SGOL1-B1-transfected cells (range, 28.6 to 37.5 minutes) compared with 25.1 minutes in the empty vector-transfected control cells (range, 20.5 to 29.6 minutes) (Figure 3d). The prolongation of the time from NEBD until anaphase onset was also observed in SGOL1-knockdown cells (range, 39.9 to 48.8 minutes; median, 44.4 minutes) (Figure 3d). These results indicate that SGOL1-B1 overexpression, as well as SGOL1-knockdown, prevent chromosomes from a proper alignment to the metaphase plate in lung cancer cells, resulting in a delay of anaphase onset.

**Association between SGOL1-B expression and the response to taxanes in NSCLC cells with WT EGFR.** Despite the recent development of various new drugs targeting specific molecules, anti-mitotic drug taxanes are still the mainstay of treatment for advanced NSCLC with WT EGFR. Since an association between the WT EGFR status and SGOL1-B expression was observed in Table 1, we examined whether the expression status of SGOL1-B was associated with the sensitivity to taxanes, such as docetaxel or paclitaxel. First, the mRNA expression levels of SGOL1-B were determined in three NSCLC cell lines with WT EGFR and a NSCLC cell line with EGFR mutation. The SGOL1-B expression levels were low in PC-3 and A549 cells

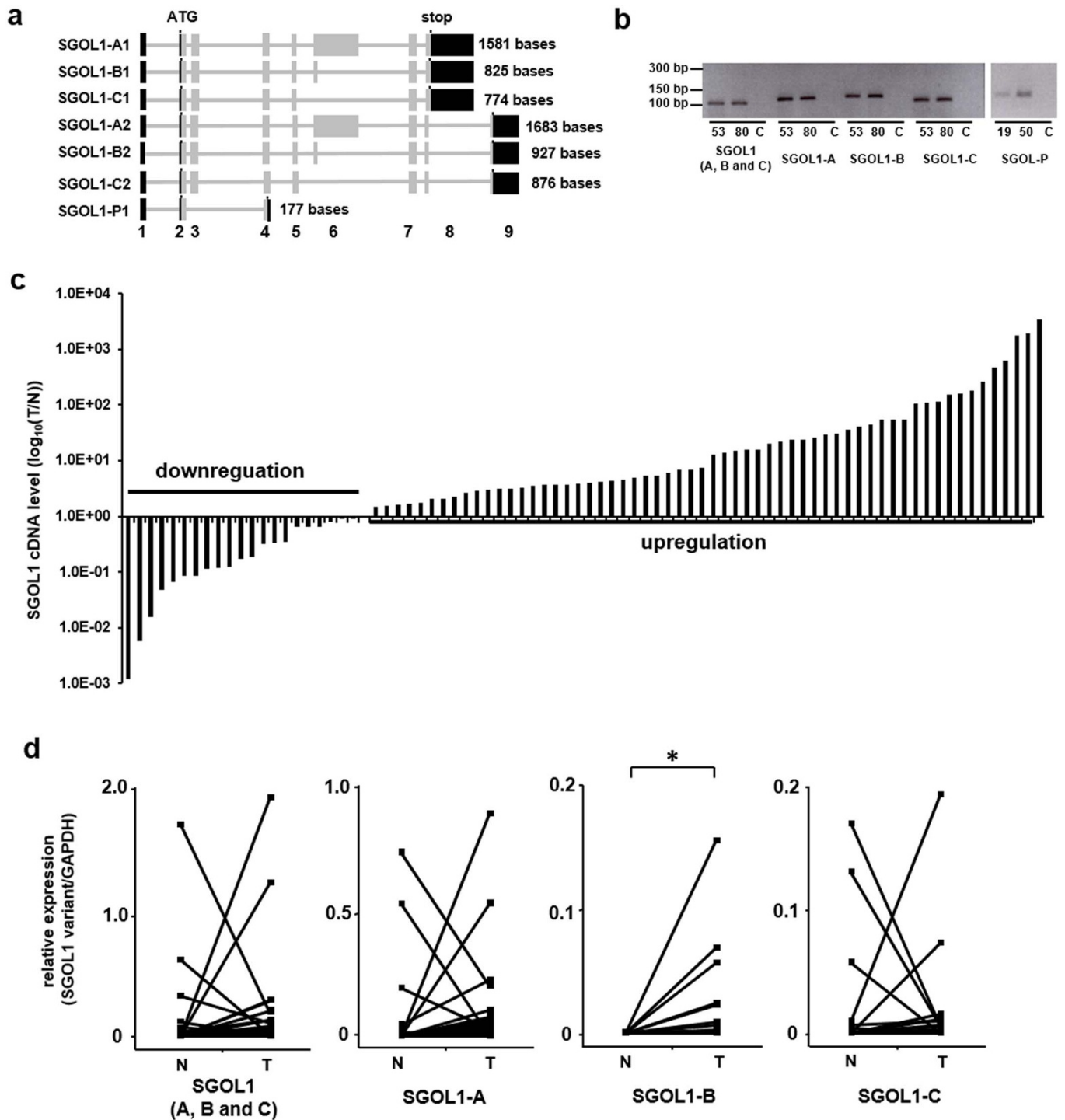


**Figure 1** | Expression of SGOL1 variants in NSCLC tissue. (a) Scheme of SGOL1 transcript variants. The filled boxes represent exons (exons 1–9). The coding region is indicated in gray, and the non-coding region is indicated in black. The number at the right indicates the length of the protein coding sequence. (b) Amplified products of various SGOL1 transcripts using quantitative real-time RT-PCR. Specific primers for each SGOL1 variant (A, B, C, and P) or primers targeting variants A, B, and C were used for the PCR. After the quantitative real-time RT-PCR reaction using a LightCycler instrument, the PCR products were electrophoresed and stained with ethidium bromide in an agarose gel to confirm the production of objective products. The number and “C” below the panel indicate the case number and negative control, respectively. (c) Measurement of the SGOL1 mRNA expression levels in 82 paired human NSCLC and normal lung tissues using quantitative real-time RT-PCR. Expression of SGOL1 transcripts containing variants A, B, and C. After normalizing the expression levels of SGOL1 to those of GAPDH, the T/N values were calculated by dividing the amount of normalized transcripts in the tumor tissue by the amount in the corresponding normal lung tissue. Cases were grouped into two categories according to their T/N value: SGOL1 downregulation ( $T/N < 1$ ) and SGOL1 upregulation ( $T/N > 1$ ). Differences between the normalized SGOL1 mRNA level in the tumor tissue and the corresponding normal tissue were statistically analyzed using the Wilcoxon matched pairs test, and the  $P$ -value was less than 0.0001. Data were calculated from triplicate measurements. (d) Paired comparison of mRNA expression from normal and tumor samples in each SGOL1 splice variant in all cases. \* $P < 0.05$  (Student  $t$ -test).



**Table 1 | Clinicopathological and molecular features of 82 NSCLC patients according to the SGOL1-B expression status in their carcinoma**

Factors	SGOL1-B expression status		P-value
	Positive n = 24 Number (%)	Negative n = 58 Number (%)	
Gender			
Male	18 (75.0%)	37 (63.8)	0.326
Female	6 (25.0%)	21 (36.2)	
Age			
Median	67	67	
Smoking			
Current/ex-smoker	22 (91.7)	40 (69.0)	0.029
Never smoker	2 (8.3)	18 (31.0)	
Pathology			
Adenocarcinoma	9 (37.5)	37 (63.8)	0.057
Squamous cell carcinoma	12 (50.0)	19 (32.8)	
Others	3 (12.5)	2 (3.4)	
Stage			
1–2	14 (58.3)	44 (75.8)	0.119
3–4	10 (41.7)	14 (24.2)	
EGFR status			
Wild-type	23 (95.8)	42 (72.4)	0.017
Mutation type*	1 (4.2)	16 (27.6)	
FGFR1 copy number			
normal	23 (95.8)	54 (93.1)	0.634
amplification	1 (4.2)	4 (6.9)	
SOX2 copy number			
normal	19 (79.2)	52 (89.7)	0.205
amplification	5 (20.8)	6 (10.3)	
PIK3CA copy number			
normal	17 (70.8)	48 (82.8)	0.226
amplification	7 (29.2)	10 (17.2)	
MET copy number			
normal	21 (87.5)	55 (94.8)	0.246
amplification	3 (12.5)	3 (5.2)	
EGFR copy number			
normal	20 (83.3)	53 (91.4)	0.289
amplification	4 (16.7)	5 (8.6)	
Focal copy number amplifications**			
negative	11 (45.8)	40 (69.0)	0.049
positive	13 (54.2)	18 (31.0)	

\*EGFR mutation type: either the exon 19 deletion or L858R point mutation in exon 21.

\*\*focal copy number amplifications were identified in at least one of the five genomic alterations (FGFR1, SOX2, PIK3CA, MET, or EGFR amplification).

compared with H1299 and ACC-LC-176 cells (Figure 4a). We next performed a growth inhibition assay to test the sensitivity of these cells to taxanes. The treatment with clinically relevant concentrations of docetaxel or paclitaxel resulted in the robust inhibition of cell viability in PC-3 and A549 cells, compared with that in H1299 and ACC-LC-176 cells (Figure 4b). This result suggests that the increased expression of SGOL1-B is associated with increased taxane resistance. Taxanes are known to promote cell death by inducing a potent mitotic block, resulting from the accumulation of cells at the G2-M phase of the cell cycle<sup>16</sup>. To further examine the morphological phenotype of cells with different SGOL1-B expression levels when exposed to 1,000 nM of docetaxel, we performed time-lapse microscopy using 4 cell lines expressing H2B-GFP fusion protein as a nuclear marker. We used the terms “death in interphase” for the processes in which the cells died in interphase before entering mitosis and “death in mitosis” for the processes in which the cells activate a death pathway while still in mitosis, according to the terminology used in a previous paper (Figure 4c and Supplementary Movie

4–5 online)<sup>17</sup>. 83.1% of the A549 cells and 72.3% of the PC-3 cells exhibited “death in interphase”, whereas the H1299 cells exhibited more variable fates, with 26.8% of the cells exhibiting “death in interphase” and 64.9% of the cells exhibiting “death in mitosis” after prophase-metaphase arrest (Figure 4d). Moreover, a substantial proportion of the ACC-LC-176 cells exhibited “death in mitosis”, indicating that they were unable to progress to cell division and died during mitosis (Figure 4d). These results suggest that the process of mitotic catastrophe caused by taxane treatment is associated with the expression level of SGOL1-B.

To exclude the possibility that differences other than the SGOL1-B expression level between A549 and ACC-LC-176 cells affect the taxane response, we examined the effect of SGOL1-B1 overexpression on taxane resistance in A549 cells. The ectopic overexpression of SGOL1-B1 enhanced the cellular viability after treatment with docetaxel or paclitaxel in A549 cells (Figure 5a). We next performed time-lapse microscopy to examine A549 cells expressing SGOL1-B1 and measured the rate of each type of cell death caused by treatment with 1,000 nM of docetaxel. Strikingly, the proportion of cells exhibiting “death in mitosis” was markedly increased by SGOL1-B1 overexpression (2.6% in control cells vs. 25.0% in cells overexpressing SGOL1-B1) (Figure 5b and Supplementary Movie 6 online). Next, we performed the knockdown of SGOL1-B in ACC-LC-176 cells to examine the role of abundant endogenous SGOL1-B. Western blotting confirmed the downregulation of SGOL1-B expression (Figure 5c). The decrease in the SGOL1-B expression level led to an increased sensitivity of ACC-LC-176 cells to docetaxel and paclitaxel (Figure 5d). Moreover, the proportion of cells exhibiting “death in interphase” after treatment with 1,000 nM of docetaxel was markedly increased by SGOL1-B1 knockdown (Figure 5e and Supplementary Movie 7 online). A similar result was obtained in H1299 cells (Supplementary Figure S1 online). These results suggest that the SGOL1-B expression level defines taxane resistance in NSCLC with WT EGFR.

## Discussion

The key findings of our study are that SGOL1 expression is upregulated in NSCLC and that the upregulation of SGOL1-B is associated with ominous clinical feature such as having WT EGFR and focal copy number amplification. SGOL1-B1 overexpression induced aberrant chromosome alignment during mitosis, the precocious separation of sister chromatids, and a delay in the onset of anaphase in lung cancer cells. Furthermore, taxane-resistance in lung cancer cells was shown to be associated with an elevated expression of SGOL1-B and mitotic arrest.

We have shown that SGOL1 was predominantly expressed in the tumorous regions of lung tissues, relative to normal tissues contrasting to the case of colon cancer, in which SGOL1 is downregulated, compared with its expression in normal tissues<sup>2</sup>. It is not surprising because gene expression patterns often differ among cancers in different organs<sup>18–21</sup>, but we do not know the implication of this difference in SGOL1 expression profile at this moment.

Genomic amplifications have long been recognized in lung cancer. Genomic profiling studies of NSCLC, using FISH, have revealed focal copy number alterations of the chromosomal area of known oncogenes, such as FGFR1 (8p12), SOX2 (3q26.3–q27), PIK3CA (3q26.3), MET (7q31.2), and EGFR (7p12.2)<sup>11–15</sup>. In our study, the profile of these genetic alterations according to different histological types of lung cancer was consistent with that of previous studies (Supplementary Table S2 online). The expression of SGOL1-B was increased specifically in lung cancer with focal copy number amplifications. Our *in vitro* studies also suggest that the overexpression of SGOL1-B in lung cancer may cause genomic instability (Supplementary Table S3 online). Thus, we hypothesized that SGOL1-B-positive cancer could be predisposed to genomic instability. The reasons for the amplifications of focal genomic areas are not known and have been

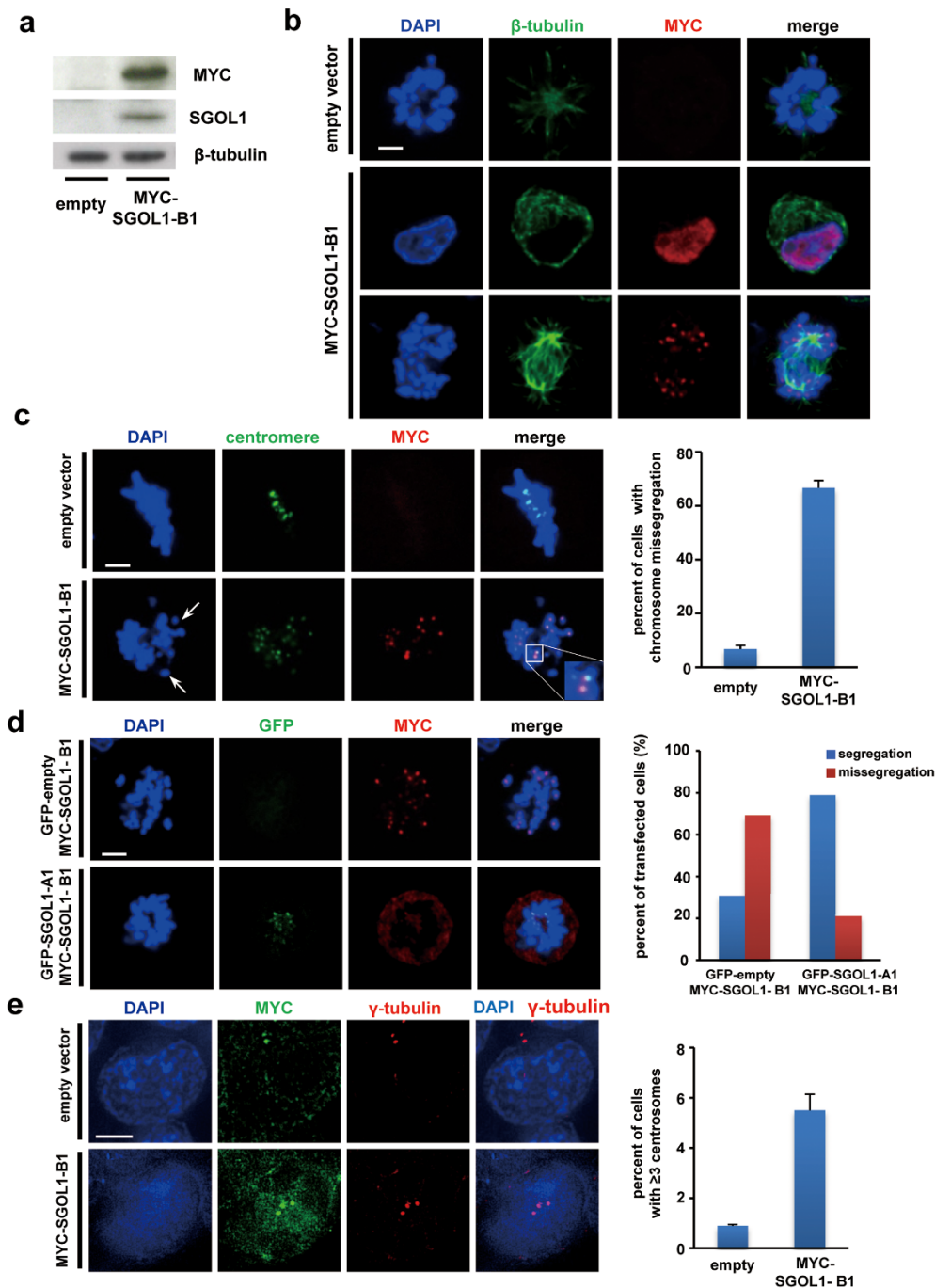


**Figure 2 | Centromeric localization and aberrant chromosome alignment during mitosis in lung cancer cells expressing SGOL1-B1.** (a) Ectopic expression of SGOL1-B1 in the human NSCLC cell line ACC-LC-176. The cells were transfected with the expression vector for MYC-SGOL1-B1, and the cellular extracts were subjected to a western blot analysis. Cropped images are shown and original whole gels and cropped lines are in Supplementary Figure S2 online. (b) Localization of SGOL1-B1 during the cell cycle. Cells at interphase (middle panels) and prophase-metaphase (lower panels) are shown using staining for MYC-SGOL1-B1 (red),  $\beta$ -tubulin (green) and DNA (blue). (c) Centromeric localization of SGOL1-B1. ACC-LC-176 cells were transfected with an empty vector or a MYC-SGOL1-B1 expression vector, and after synchronization to metaphase using nocodazole, the cells were stained with an anti-MYC antibody (red), anti-centromere antibody (green) and DAPI (blue). The inset shows a magnified image of the centromere. The mitotic cell expressing MYC-SGOL1-B1 (lower panels) shows chromosome missegregation. An attached graph shows percentage of cells exhibiting chromosome missegregation. The results are presented as ( $n = 50$ ) from three independent experiments. (d) Rescue of SGOL1-B1-derived missegregation phenotype by the overexpression of SGOL1-A1 in NSCLC cells. ACC-LC-176 cells were transfected with GFP-empty or GFP-SGOL1-A1 vector together with the MYC-SGOL1-B1 expression vector. At 20 h post-transfection, the cells were synchronized to metaphase with nocodazole, fixed, and stained with an anti-MYC antibody (red) and DAPI (blue). Chromosome missegregation is shown in the upper panels, while the chromosomes were properly segregated in the lower panels. Scale bar = 5  $\mu$ m. Statistical analysis of misaligned chromosomes in experiment. Results are presented ( $n = 50$ ) from three independent experiments. (e) Centrosome amplification detected in ACC-LC-176 cells expressing SGOL1-B1. The cells were transfected with an empty vector or a MYC-SGOL1-B1 expression vector, and at 48 h post-transfection, the cells were stained with an anti-MYC antibody (green), anti- $\gamma$ -tubulin (red), and DAPI (blue). Scale bar = 5  $\mu$ m. An attached graph shows percentage of cells exhibiting centrosome amplification. Results are presented ( $n = 200$ ) from three independent experiments.

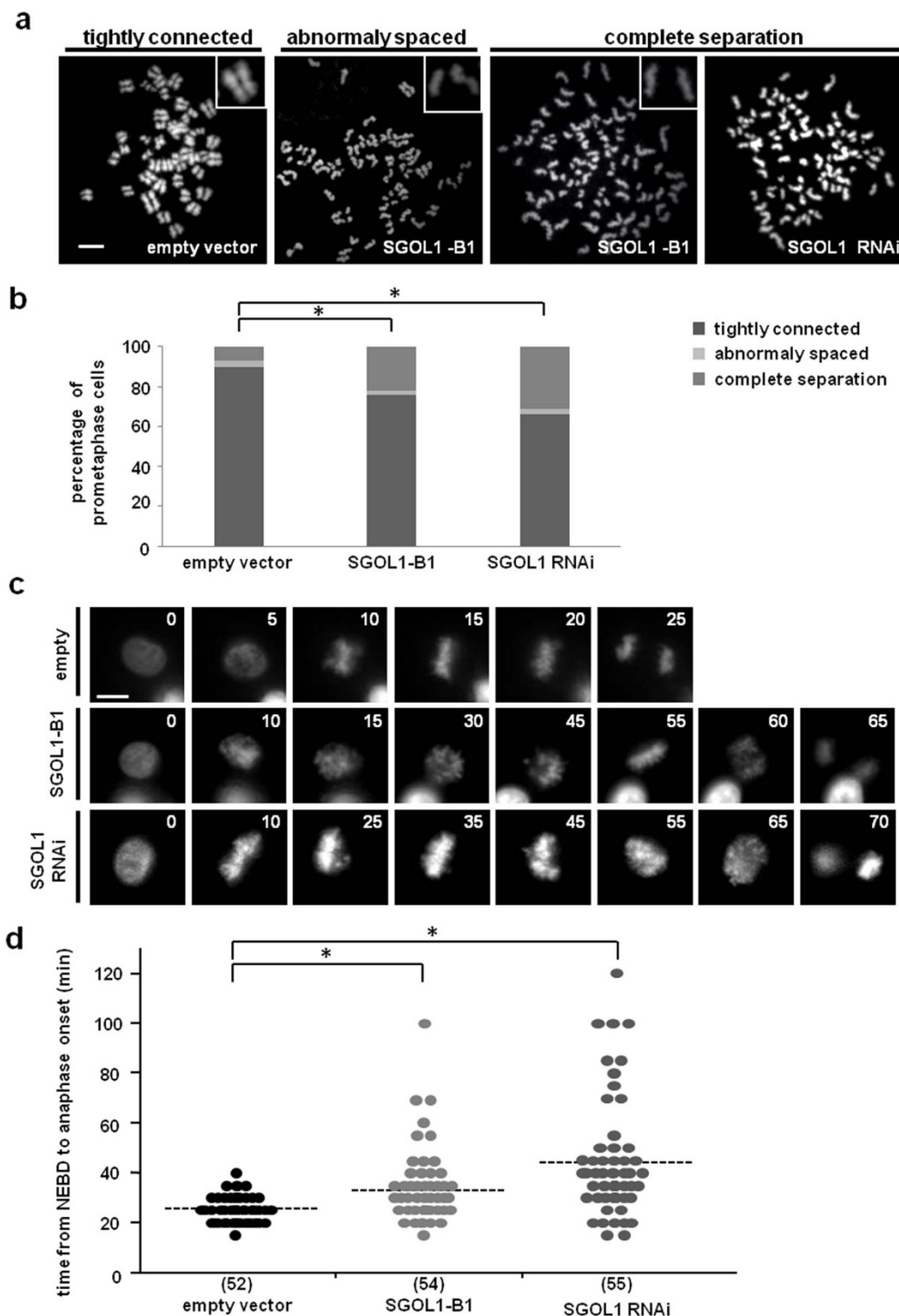


**Figure 3 | Cohesion defects between sister chromatids and delayed mitotic progression in lung cancer cells expressing SGOL1-B1.** (a) Representative images of chromosome spread exhibiting cohesion defects. The NSCLC cell line ACC-LC-176 was transfected with GFP-H2B expression vector together with the MYC-SGOL1-B1 expression vector, SGOL1 shRNA vector, or control vector. The cells were then treated with nocodazole to arrest the cell cycle during mitosis, and the chromosomes were spread, stained with DAPI, and classified into the following three patterns: (I) tightly connected pattern, normal cohesive chromatids or only a very few pairs of separated sister chromatids; (II) abnormally spaced pattern, separated chromatids have remained in close proximity to the pair partner (several chromatid pairs remain cohesive); and (III) complete separation pattern, severely separated chromatids (the pair partner is often hard to identify because it is located some distance away). (b) Percentage of cells with cohesion defects between sister chromatids in experiment (a).  $*P < 0.05$  (Fisher exact test). (c) Detection of delayed mitotic progression in ACC-LC-176 cells transfected with vectors as described in (a) using time-lapse analysis. The mitotic progression time was defined as the elapsed time from NEBD to anaphase onset. Images were acquired every 5 min. The elapsed time in minutes is shown at the upper right of each panel. Scale bar = 10  $\mu$ m. (d) Quantitation of the mitotic progression time in experiment (c). Each symbol in the scatter plot represents a single cell. The solid horizontal bars represent the median values.  $*P < 0.0005$  [Mann-Whitney *U*-test]. The numbers of examined cells are indicated in parentheses.

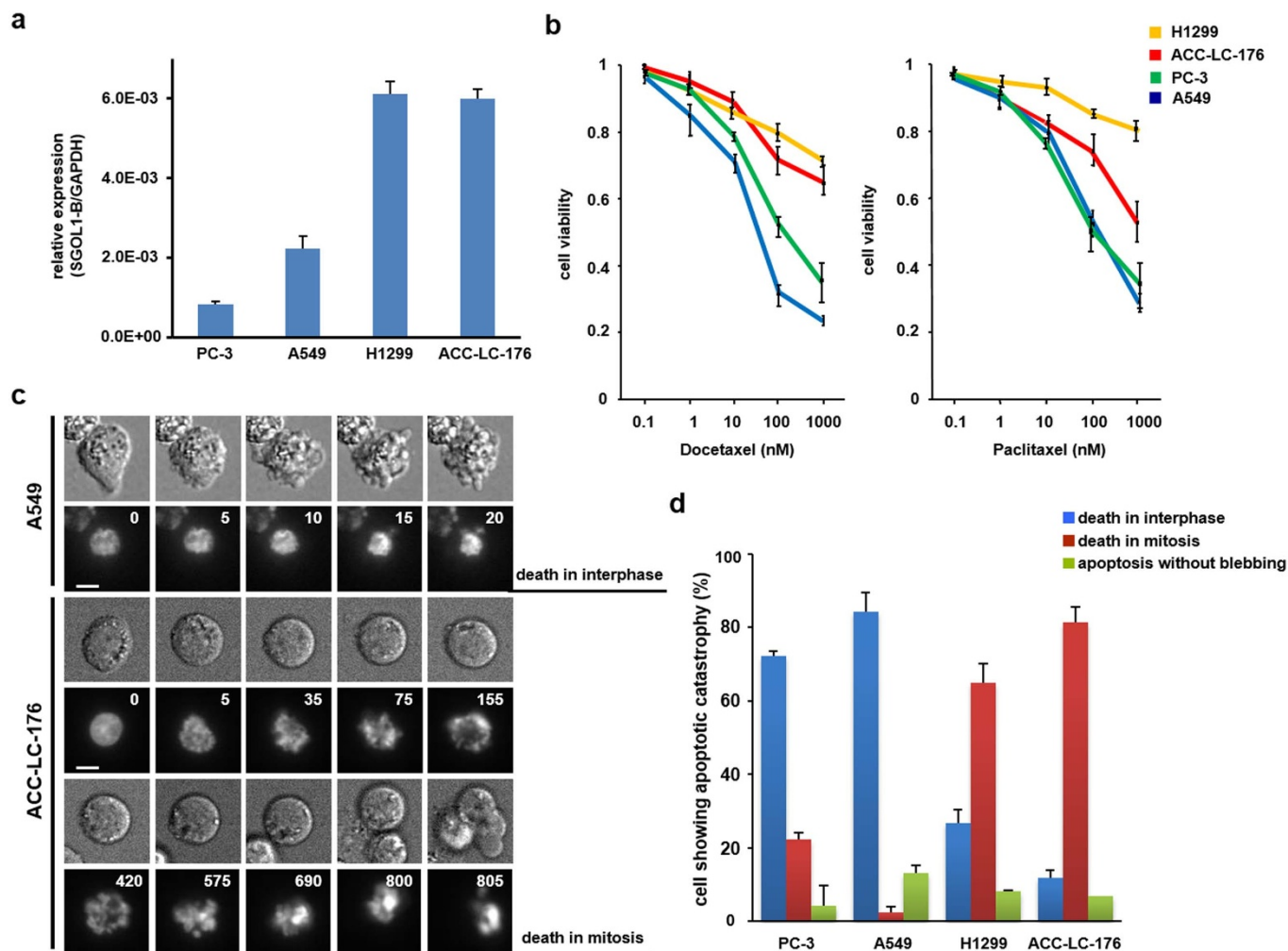


**Figure 4 | Difference in taxane responses of WT EGFR NSCLC cell lines according to their SGOL1-B expression level.** (a) SGOL1-B mRNA expression levels determined using quantitative real-time RT-PCR in three NSCLC cell lines with WT EGFR and a cell line with EGFR mutation. The data shown are the mean of at least three independent experiments. (b) Responses of PC-3, A549, H1299 and ACC-LC-176 cells to docetaxel and paclitaxel treatment as evaluated using a WST-8 colorimetric assay. (c) Representative images of time-lapse sequences illustrating the two types of death after exposure to docetaxel. Scale bar = 10  $\mu$ m. The number at the upper right of each panel indicates the time in minutes. (d) Percentages of PC-3, A549, H1299 and ACC-LC-176 cells exhibiting various cell fates in response to 1,000 nM of docetaxel.

sparsely addressed in previous literature. Our observation may imply that a guardian of mitosis control and its aberrant spliced product may bring about global instability in the genome, causing the amplification of particularly sensitive regions of the chromosomes<sup>22,23</sup>.

Our present study revealed a new and important role of SGOL1-B in lung cancer progression. The overexpression of SGOL1-B has been associated with centrosome amplification. Multiple spindle poles have been reported to be common in mitotic SGOL1-knockdown cells and the cell expressing SGOL1-P1<sup>2,4,24</sup>. In a lung cancer cell line transfected with SGOL1-B, considerable amount of centrosome amplification was noted. Several studies have demonstrated a relationship between exposure to carcinogens implicated in lung cancer and the development of centrosome abnormalities *in vitro*<sup>25,26</sup>. SGOL1 is required for the protection of centromeric cohesion from prophase to the metaphase-anaphase transition until all the kinetochores have been properly captured by the spindle microtubules<sup>27</sup>. In SGOL1-B1 overexpressed cells, the weakness of centromere protection induces accurate chromosome missegregation on the metaphase plate, leading to mitotic delay. This result is consistent with the observation that cells expressing SGOL1-B showed a high frequency of mitotic cells with premature centromere separation that were delayed at the G2/M transition<sup>3</sup>. Cells with SGOL1-B overexpression,

which showed a cancer tissue-specific expression in primary lung cancer, induced aberrant mitosis, which accelerated the acquisition of further malignant phenotypes. On the other hand, in terms of concurrent centrosome amplification associated with SGOL1-B overexpression as described above, centrosome proteins like PLK4 and Tpx2 are also known to be involved with generation of aberrant mitosis, the same phenotype shown here. Actually, a high frequency of mitotic errors are notable in lung cancer cells spontaneously occurring in mice heterozygous for PLK4 and Tpx2<sup>28,29</sup>. Our study showing that the overexpression of SGOL1-B is observed in lung cancer provides a new and important link between aberrant mitosis and lung carcinogenesis.

Taxanes are among the most widely used antitumor agents in the treatment of NSCLC. Our data clearly showed that SGOL1-B upregulation was associated with a more intractable subset of NSCLC. A lung cancer cell line that overexpressed SGOL1-B exhibited an aberrant dynamicity in response to taxanes. Taxanes successfully kill tumor cells during mitosis by targeting microtubules and disrupting normal chromosome movement<sup>30</sup>. This effect occurs because the primary effect of taxanes is to bind to microtubules, thereby decreasing mitotic dynamicity. Thus, this cell line expressing SGOL1-B is thought to be more prone to overcoming the effects of taxanes on

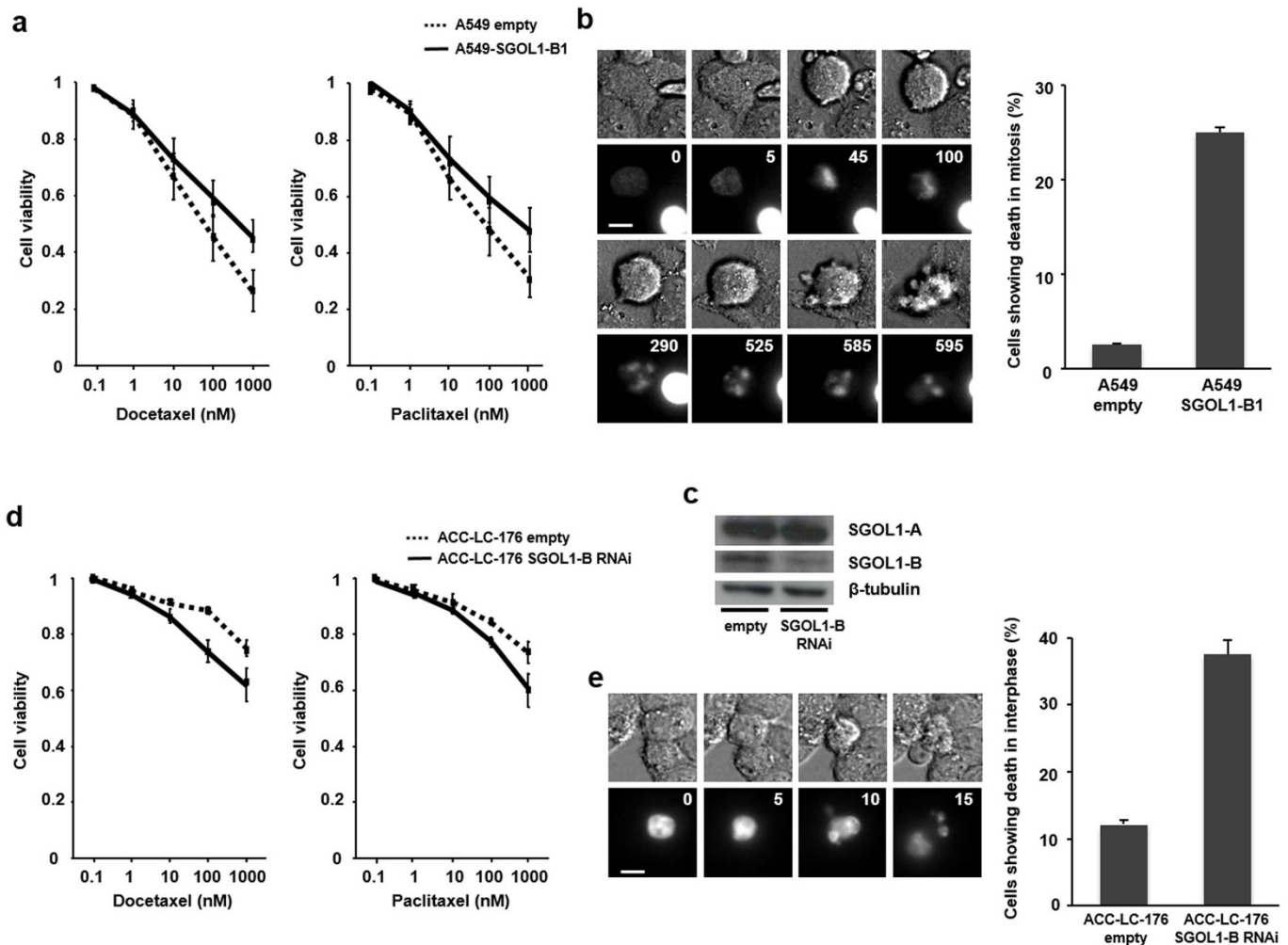


**Figure 5 | Expression level of SGOL1-B defines the response to docetaxel.** (a) Responses of empty vector (mock)- and SGOL1-B1-transfected A549 NSCLC cells to docetaxel and paclitaxel as evaluated using a WST-8 colorimetric assay. The data shown are the mean of at least three independent experiments. (b) Representative images of “death in mitosis” in A549 cells overexpressing SGOL1-B1 detected using time-lapse microscopy. Scale bar = 10  $\mu$ m. An attached graph shows percentages of mock- and SGOL1-B1 expression vector-transfected A549 cells exhibiting “death in mitosis” in response to 1,000 nM of docetaxel. (c) Western blot analysis of expression of SGOL1-B in ACC-LC-176 NSCLC cells after shRNA knockdown for SGOL1-B was inside the graph. Cropped images are shown and the original whole gels are available in Supplementary Figure S3 online. (d) Responses of mock vector- and SGOL1-B shRNA expression vector-transfected ACC-LC-176 cells to docetaxel and paclitaxel as evaluated using a WST-8 colorimetric assay. The data shown are the mean of at least three independent experiments. (e) Representative images of “death in interphase” of SGOL1-B-knockdown ACC-LC-176 cells detected using time-lapse microscopy. Scale bar = 10  $\mu$ m. An attached graph shows percentages of mock- and SGOL1-B shRNA expression vector-transfected ACC-LC-176 cells exhibiting “death in interphase” in response to 1,000 nM of docetaxel.

microtubule dynamics. It is tempting to speculate that the assessment of SGOL1-B expression might be a predictive marker for taxane-based chemotherapy. Until now, several markers are proposed as predictors of responses to taxane therapy<sup>31,32</sup>. Especially, high levels of  $\beta$ III-tubulin expression in NSCLC are associated with low response rates and poorer survival in patients treated with chemotherapies based on anti-mitotic agents<sup>33–35</sup>. Our data indicate that a taxane-resistant lung cancer cell line expresses higher mRNA levels of a specific SGOL1 splice variant, SGOL1-B. The determination of the SGOL1-B mRNA level may be useful for selecting subjects who are likely to benefit from chemotherapy based on taxanes.

The molecular pathways resulting in taxane-induced cell death without mitosis entry (“death in interphase”) or death in response to aberrant mitosis (“death in mitosis”) remain unclear<sup>17,36</sup>. In our study, lung cancer cells with a high expression level of SGOL1-B were more resistant to mitotic arrest induced by taxane than other cell lines with a low expression level of SGOL1-B. Although mitotic arrest is a hallmark cellular response to taxane, previous studies have shown

that the antitumor efficacy of paclitaxel is dependent on its ability to induce apoptosis, not mitotic arrest<sup>37</sup>. Another study with NSCLC A549 cells also found that low concentrations of paclitaxel are sufficient to induce cell death without an apparent G2-M block<sup>38</sup>. These reports strongly support our result that A549, which had a low expression level of SGOL1-B, was taxane-sensitive. The expression level of SGOL1-B may alter cellular fate profiles.

We do not know exactly what produced the multitude of genetic changes in lung cancer cases with SGOL1-B overexpression. Our analysis may provide an insight that abnormal mitosis in response to an elevated SGOL1-B level posits the cancer cells as having a high frequency of focal copy number amplifications. NSCLC cells with a high expression level of SGOL1-B that were exposed to taxane underwent mitotic arrest. The mechanism of taxane-resistance might be associated with abnormal mitosis induced by SGOL1-B and mitotic arrest induced by taxane. These findings underlie the importance of determining the SGOL1-B expression status, which could be used in addition to the EGFR status in the selection of candidates for





taxane-based chemotherapy. We are even tempted to expect that the manipulative downregulation of SGOL1-B may increase the sensitivity of the cancer cells to taxane.

## Methods

All experiments were performed in accordance with relevant guidelines and regulations. All the study protocols were approved by the Institutional Review Board of Hamamatsu University School of Medicine (reference number 23–91).

**Tissue samples and nucleic acid extraction.** Tissues from patients with primary NSCLC were surgically resected at the Hamamatsu University Hospital (Japan), Shimada Municipal Hospital (Japan), and Seirei Mikatahara General Hospital (Japan). Written informed consent was obtained from all subjects. Total RNA and genomic DNA were extracted from the tumors and normal tissues using the commercially available ISOGEN kit (Nippongene, Tokyo, Japan) and the DNeasy Tissue kit (QIAGEN, Valencia, CA, USA), according to the manufacturers' instructions. The tumor tissues were examined for somatic mutations in mutation cluster regions (hot spots) of the *EGFR* gene. The primers used for PCR and DNA sequencing have been described previously<sup>39</sup>. The study design was approved by the Institutional Review Boards of the relevant hospitals.

**Quantitative real-time RT-PCR and plasmid construction.** The structure and nomenclature of the transcripts of SGOL1 is shown in Figure 1a. Isoform SGOL1-B does not contain part of exon 6. We measured SGOL1-B, including both SGOL1-B1 and SGOL1-B2, using common primers. For the *in vitro* experiments, we used a construct of SGOL1-B1 containing exon 8.

Quantitative real-time RT-PCR was performed as described in our previous report<sup>2</sup>. The primer sequences used for the first RT-PCR for SGOL1 (Figure 1b) were as follows: forward, 5'-GACCCCAATAGTGATGACAGC-3', reverse, 5'-GAAATGATTCTCCTTGTCTGG-3'. For the amplification of each SGOL1 variant, the following primer sequences were used: the common forward primer for SGOL1-A, -B, and -C was 5'-CTCCAGAAATTTATTTGTGAAGG-3', and the reverse primers for SGOL1-A, -B, and -C were 5'-CAAAATCAACTCCCAGTGTGTC-3', 5'-GGTGGTGTAGCTGAATCAAATC-3', and 5'-GTTTCAGGTGGTGTAGCTTCTATTG-3', respectively. The *Glyceraldehyde-3-phosphate dehydrogenase* (*GAPDH*) transcript was amplified as an internal control, as described previously<sup>2</sup>. To express SGOL1-B1 in mammalian cells, three MYC tag sequences were fused to the 5'-side of SGOL1-B1 using PCR amplification, and the product was inserted into a pIRESpuo2 expression vector (Clontech, Palo Alto, CA, USA). A pSilencer plasmid with short hairpin RNA (shRNA) targeting the total SGOL1 and SGOL1-B sequences was used for the RNA interference (RNAi) procedure, as described previously<sup>2</sup>. The SGOL1-B shRNA expression vector was constructed by inserting shRNA sequences targeting SGOL1-B (target sequence: 5'-GATTCAGCTACACCACCTGA-3') into pSilencer 2.1-U6 puro (Applied Biosystems, Tokyo, Japan).

**Fluorescence *in situ* hybridization (FISH) analysis.** FISH analysis was performed on FFPE tumor samples and cell lines according to the manufacturers' instructions with minor modifications, as described previously<sup>40,41</sup>. Spectrum Orange-labeled BAC clones, RP11-106B16 (8p12, FGFR1), RP11-245 + RP11-355N16 (3q26.3, PIK3CA), RP11-275H4 (3q26.3, SOX2), RP11-51M22 (7q31.1, MET), and RP5-1091E12 (7q12, EGFR) (Advanced Genotechs Co., Tsukuba, Japan), were used as locus-specific FISH probes. Spectrum Green-labeled control probes for the near centromere locus on chromosome 3 (RP11-91A15), 7 (RP11-90C3), and 8 (RP11-12L15) (Advanced Genotechs Co.) were also used to enumerate the copies of chromosome 3, 7, and 8 in the FISH experiments. 4',6-Diamidino-2-phenylindole (DAPI) (Vector Laboratories, Burlingame, CA, USA) was used for nuclear staining. At least 50 tumor cell nuclei were counted per case. Copy number amplification was defined by a BAC signal/CEP signal ratio greater than or equal to 2.0 or the presence of a tight gene cluster.

**Cell culture and transfection.** The human NSCLC cell lines A549 (adenocarcinoma), PC-3 (adenocarcinoma), H1299 (large cell carcinoma) and ACC-LC-176 (squamous cell carcinoma) were cultured at 37°C in RPMI medium (Invitrogen, Carlsbad, CA, USA) containing 5% or 10% fetal bovine serum (Nichirei, Tokyo, Japan) under 5% CO<sub>2</sub>. The A549 and H1299 cell lines were gifts from Dr. Niki (Jichi Medical University), and the ACC-LC-176 cell line was a gift from Dr. Takahashi (Nagoya University). Transfection was performed using a Lipofectamine 2000 reagent (Invitrogen) according to the manufacturer's protocol.

**Antibodies.** Rabbit polyclonal anti-shugoshin (ab21633; Abcam, Cambridge, MA, USA) and anti-MYC tag (06-549; MILLIPORE, Bedford, MA, USA) antibodies and mouse monoclonal anti-β-tubulin (2-28-33; Sigma, St. Louis, MO, USA), anti-γ-tubulin (GTU88; Sigma), and anti-shugoshin (ab58023; Abcam) antibodies were used for western blotting and immunofluorescence staining as primary antibodies. A human autoantibody against the centromere (Immunovision, Springdale, AR, USA) was used for the immunofluorescent staining of the kinetochores. HRP-conjugated donkey polyclonal anti-rabbit antibody or anti-mouse IgG antibody (GE Healthcare, Piscataway, NJ, USA) and Alexa Fluor 488/546/633-conjugated goat polyclonal anti-rabbit, anti-mouse or anti-human IgG antibodies (Invitrogen) were used as secondary antibodies.

**Western blotting.** Cells were washed with PBS (-) and lysed with lysis buffer. The protein concentration of the lysate was measured using a BCA protein assay kit (Thermo Scientific, Rockford, IL, USA). Following the addition of sodium dodecyl sulfate (SDS) sample buffer, the samples were boiled, and ten micrograms of the cell lysate were subjected to SDS polyacrylamide gel electrophoresis. The electrophoresed proteins were then transferred to a membrane, and the protein of interest was detected using appropriate antibodies and the ECL Western Blotting Detection System (GE Healthcare), as described previously<sup>42</sup>.

**Indirect immunofluorescence analysis.** Cells were washed with PBS and fixed with 4% paraformaldehyde at room temperature for 15 min or in methanol at -20°C for 5 min. After permeabilization and subsequent incubation with 10% normal goat serum blocking solution, the cells were probed with primary antibody. Indirect immunofluorescence labeling was then performed by exposure to Alexa Fluor-conjugated secondary antibody (Molecular Probes, Eugene, OR, USA), and the nuclei were stained with DAPI. The immunostained cells were examined under a confocal laser scanning microscope (FV1000; Olympus, Tokyo, Japan) or a fluorescence microscope (BZ-9000; KEYENCE, Osaka, Japan).

**Chromosome spread.** Transfected cells were selected with puromycin for 48 h and treated with 100 nM nocodazole (Sigma) for 20 h. They were then trypsinized and collected by centrifugation in a conical tube. The cells were gently suspended with hypotonic solution (75 mM KCl) and incubated at 37°C for 6 min. Chilled fixative solution (methanol/glacial acetic acid, 3:1) was gently added to the cells that had been collected by centrifugation, and this procedure consisting of centrifugation, cell collection, and the addition of chilled fixative solution was repeated three times. The fixed cells were dropped onto the slide glasses. After drying in air, they were stained with DAPI.

**Time-lapse imaging.** Cells were transfected with a total of 1 μg of expression vector for histone H2B-green fluorescent protein (GFP) together with an empty vector, the MYC-SGOL1-B1 expression vector, or the shRNA vector (molar ratio, 1:5). Docetaxel was then added to the growth medium of the control cells or the targeted shRNA-treated cells at 72 h after transfection (Figure 4c, 5b and 5e). After 48 h of culture, the medium was replaced with fresh medium and the cells were subjected to time-lapse imaging (FCV100; Olympus) using a device equipped with an incubation chamber. Fluorescence signals from the GFP were captured at 5-min intervals for 24 h, and the data were used to prepare a montage of images and movies. The image sequences were viewed using ImageJ software (version 1.43f; National Institutes of Health, Bethesda, MD, USA).

**Growth inhibition assay.** Cytotoxicity was evaluated using a WST-8 [2-(2-methoxy-4-nitrophenyl)-3-(4-nitrophenyl)-5-(2,4-disulphophenyl)-2H tetrazolium, monosodium salt] colorimetric assay. Cancer cells (5,000 cells/well) were seeded into 96-well cell plates in 100 μL of culture medium for 24 h before drug exposure. The cells were then treated with various concentrations of paclitaxel and docetaxel for 24 h. After drug exposure, the medium was discarded and replaced with 90 μL of fresh medium followed by the addition of 10 μL of WST-8 reagent solution (Cell Counting Kit; Dojindo Laboratories, Kumamoto, Japan) and incubated for 2 h at 37°C. Cell viability was determined by colorimetric comparison by reading the optical density values from a microplate reader at an absorption wavelength of 450 nm, according to the manufacturer's instructions.

**Statistical analysis.** The Mann-Whitney *U*-test was used to statistically analyze non-parametric data. The chi-square test or Fisher exact test was used to compare categorical variables. Differences in continuous variables were analyzed using the Student *t*-test for comparing 2 groups and using an ANOVA for multiple groups. Comparisons with *P* < 0.05 were considered statistically significant. The statistical analysis was performed using JMP software, version 7.0.1J (SAS Institute Japan, Tokyo, Japan).

- Kitajima, T. *et al.* Shugoshin collaborates with protein phosphatase 2A to protect cohesin. *Nature* **441**, 46–52 (2006).
- Iwaizumi, M. *et al.* Human Sgo1 downregulation leads to chromosomal instability in colorectal cancer. *Gut* **58**, 249–260 (2009).
- Suzuki, H. *et al.* Human Shugoshin mediates kinetochore-driven formation of kinetochore microtubules. *Cell Cycle* **5**, 1094–1101 (2006).
- Kahyo, T. *et al.* A novel tumor-derived SGOL1 variant causes abnormal mitosis and unstable chromatid cohesion. *Oncogene* **30**, 4453–4463 (2011).
- Jemal, A., Siegel, R., Xu, J. & Ward, E. Cancer statistics. *CA Cancer J Clin.* **60**, 277–300 (2010).
- Lynch, T. J. *et al.* Activating mutations in the epidermal growth factor receptor underlying responsiveness of non-small-cell lung cancer to gefitinib. *N Engl J Med* **350**, 2129–2139 (2004).
- Soda, M. *et al.* Identification of the transforming EML4-ALK fusion gene in non-small-cell lung cancer. *Nature* **448**, 561–566 (2007).
- Shinmura, K. *et al.* EML4-ALK fusion transcripts, but no NPM-, TPM3-, CLTC-, ATIC-, or TFG-ALK fusion transcripts, in non-small cell lung carcinomas. *Lung Cancer* **61**, 63–169 (2008).
- Belani, C. P. *et al.* Randomized, phase III study of weekly paclitaxel in combination with carboplatin versus standard every-3-weeks administration of carboplatin



- and paclitaxel for patients with previously untreated advanced non-small-cell lung cancer. *J Clin Oncol* **26**, 468–473 (2008).
10. Weaver, B. A. & Cleveland, D. W. Decoding the links between mitosis, cancer, and chemotherapy: The mitotic checkpoint, adaptation, and cell death. *Cancer Cell* **8**, 7–12 (2005).
  11. Weiss, J. *et al.* Frequent and focal FGFR1 amplification associates with therapeutically tractable FGFR1 dependency in squamous cell lung cancer. *Sci Transl Med.* **2**, 62ra93 (2010).
  12. Bass, A. J. *et al.* SOX2 is an amplified lineage-survival oncogene in lung and esophageal squamous cell carcinomas. *Nat Genet.* **41**, 1238–1242 (2009).
  13. Okudela, K. *et al.* PIK3CA mutation and amplification in human lung cancer. *Pathol Int.* **57**, 664–671 (2007).
  14. Cappuzzo, F. *et al.* Increased MET gene copy number negatively affects survival of surgically resected non-small-cell lung cancer patients. *J Clin Oncol.* **27**, 1667–1674 (2009).
  15. Tsao, M. S. *et al.* Erlotinib in lung cancer - molecular and clinical predictors of outcome. *N Engl J Med.* **353**, 133–144 (2005).
  16. Jordan, M. A. & Wilson, L. Microtubules and actin filaments: dynamic targets for cancer chemotherapy. *Curr Opin Cell Biol.* **10**, 123–130 (1998).
  17. Gascoigne, K. E. & Taylor, S. S. Cancer cells display profound intra- and interline variation following prolonged exposure to antimetabolic drugs. *Cancer Cell* **14**, 111–122 (2008).
  18. Kitamura, S. *et al.* Peroxisome proliferator-activated receptor gamma induces growth arrest and differentiation markers of human colon cancer cells. *Jpn J Cancer Res.* **90**, 75–80 (1999).
  19. Chang, T. H. & Szabo, E. Induction of differentiation and apoptosis by ligands of peroxisome proliferator-activated receptor  $\gamma$  in non-small cell lung cancer. *Cancer Res.* **60**, 1129–1138 (2000).
  20. Passeron, T. *et al.* Upregulation of SOX9 inhibits the growth of human and mouse melanomas and restores their sensitivity to retinoic acid. *J Clin Invest.* **119**, 954–963 (2009).
  21. Jiang, S. S. *et al.* Upregulation of SOX9 in lung adenocarcinoma and its involvement in the regulation of cell growth and tumorigenicity. *Clin Cancer Res.* **16**, 4363–4373 (2010).
  22. Watanabe, Y., Ikemura, T. & Sugimura, H. Amplicons on human chromosome 11q are located in the early/late-switch regions of replication timing. *Genomics* **84**, 796–805 (2004).
  23. Duijff, P. H. & Benezra, R. The cancer biology of whole-chromosome instability. *Oncogene* **32**, 1–10 (2013).
  24. Dai, J., Kateneva, A. V. & Higgins, J. M. Studies of haspin-depleted cells reveal that spindle-pole integrity in mitosis requires chromosome cohesion. *J Cell Sci.* **122**, 4168–4176 (2009).
  25. Shinmura, K. *et al.* Induction of centrosome amplification and chromosome instability in p53-deficient lung cancer cells exposed to benzo[a]pyrene diol epoxide (B[a]PDE). *J Pathol.* **216**, 365–374 (2008).
  26. Xie, H. *et al.* Neoplastic transformation of human bronchial cells by lead chromate particles. *Am J Respir Cell Mol Biol.* **37**, 544–552 (2007).
  27. Watanabe, Y. Shugoshin: guardian spirit at the centromere. *Curr Opin Cell Biol.* **17**, 590–595 (2005).
  28. Ko, M. A. *et al.* Plk4 haploinsufficiency causes mitotic infidelity and carcinogenesis. *Nat Genet.* **37**, 883–888 (2005).
  29. Aguirre-Portoles, C. *et al.* Tpx2 controls spindle integrity, genome stability, and tumor development. *Cancer Res.* **72**, 1518–1528 (2012).
  30. Zelnak, A. B. Clinical pharmacology and use of microtubule-targeting agents in cancer therapy. *Methods Mol Med.* **137**, 209–234 (2007).
  31. Yerushalmi, R., Woods, R., Ravdin, P. M., Hayes, M. M. & Gelmon, K. A. Ki67 in breast cancer: prognostic and predictive potential. *Lancet Oncol.* **11**, 174–183 (2010).
  32. Honma, K. *et al.* RPN2 gene confers docetaxel resistance in breast cancer. *Nat Med.* **14**, 939–948 (2008).
  33. Gan, P. P., Pasquier, E. & Kavallaris, M. Class III  $\beta$ -tubulin mediates sensitivity to chemotherapeutic drugs in non small cell lung cancer. *Cancer Res.* **67**, 9356–9363 (2007).
  34. Seve, P. *et al.* Class III  $\beta$ -tubulin expression in tumor cells predicts response and outcome in patients with non-small cell lung cancer receiving paclitaxel. *Mol Cancer Ther.* **4**, 2001–2007 (2005).
  35. Vilmar, A. C., Santoni-Rugiu, E. & Sorensen, J. B. Class III beta-tubulin in advanced NSCLC of adenocarcinoma subtype predicts superior outcome in a randomized trial. *Clin Cancer Res.* **17**, 5205–5214 (2011).
  36. Janssen, A. & Medema, R. H. Mitosis as an anti-cancer target. *Oncogene* **30**, 2799–2809 (2011).
  37. Milross, C. G. *et al.* Relationship of mitotic arrest and apoptosis to antitumor effect of paclitaxel. *J Natl Cancer Inst.* **88**, 1308–1314 (1996).
  38. Torres, K. & Horwitz, S. B. Mechanisms of Taxol-induced cell death are concentration dependent. *Cancer Res.* **58**, 3620–3626 (1998).
  39. Davies, H. *et al.* Somatic mutations of the protein kinase gene family in human lung cancer. *Cancer Res.* **65**, 7591–7595 (2005).
  40. Sugimura, H. Detection of chromosome changes in pathology archives: an application of microwave-assisted fluorescence in situ hybridization to human carcinogenesis studies. *Carcinogenesis* **29**, 681–687 (2008).
  41. Sugimura, H. *et al.* Fluorescence in situ hybridization analysis with a tissue microarray: ‘FISH and chips’ analysis of pathology archives. *Pathol Int.* **60**, 543–550 (2010).
  42. Shinmura, K. *et al.* Reduced expression of MUTYH with suppressive activity against mutations caused by 8-hydroxyguanine is a novel predictor of a poor prognosis in human gastric cancer. *J Pathol.* **225**, 414–423 (2011).

## Acknowledgments

We are grateful to Dr. Niki (Jichi Medical University, Shimotsuke, Japan) for providing us with a lung cancer cell line. We also acknowledge Mrs. K. Nagura, Mr. T. Kamo and Mr. S. Kageyama (Hamamatsu University School of Medicine) for their technical assistance. We appreciate Dr. Shuji Ogino (Brigham and Women’s Hospital) and Dr. Mari Iida and Dr. Roger Wiseman (University of Wisconsin) for a critical reading of the manuscript. This work was supported by grants from the Ministry of Health, Labour and Welfare (19–19, 10103838), the Japan Society for the Promotion of Science (22590356, 23790396), Ministry of Education, Culture, Sports, Science and Technology (S-001), National Cancer Center Research and Development Fund, and the Smoking Research Foundation.

## Author contributions

S.M. performed and designed the experiments, T.K., K.S., M.I. and H.Y. prepared the plasmid constructs, antibodies, and cells. K.F., J.K., M.T., H.N., H.O., N.I., T.S., H.S. and K.C. provided clinico-pathological data and analyses. T.K., K.S., M.I., T.T. and Y.W. input the discussion and arguments from the standpoint of cell biology. S.M., T.K., K.S., and H.S. wrote the manuscript. H.S. conceived the whole plan integrating clinicals, FISH analyses, and in vitro scheme. All the authors reviewed the manuscript.

## Additional information

**Supplementary information** accompanies this paper at <http://www.nature.com/scientificreports>

**Competing financial interests:** The authors declare no competing financial interests.

**How to cite this article:** Matsuura, S. *et al.* SGOL1 variant B induces abnormal mitosis and resistance to taxane in non-small cell lung cancers. *Sci. Rep.* **3**, 3012; DOI:10.1038/srep03012 (2013).



This work is licensed under a Creative Commons Attribution-NonCommercial-ShareAlike 3.0 Unported license. To view a copy of this license, visit <http://creativecommons.org/licenses/by-nc-sa/3.0>